Pharmacy Reports

https://doi.org/10.51511/pr.127

ORIGINAL ARTICLE

Open Access

Network pharmacology and molecular docking of cucurbitane-type triterpenoids from *Momordica charantia* against psoriasis-associated targets

Ahmad Bayu Satriawan, Sarmoko*, Tantri Liris Nareswari, Nisa Yulianti Suprahman, Muh Fajar Fauzi, I Gede Raditya Purwanata

Department of Pharmacy, Faculty of Science, Institut Teknologi Sumatera, South Lampung 25365, Lampung, Indonesia

*Corresponding author: Jl. Terusan Ryacudu, Way Hui, Jati Agung, South Lampung 35365, Lampung, Indonesia.

Email: sarmoko@fa.itera.ac.id

Abstract: Psoriasis is a chronic immune-mediated inflammatory skin disorder characterized by keratinocyte hyperproliferation, persistent inflammation, dysregulated apoptosis, and tissue remodeling. *Momordica charantia* has attracted attention as a potential anti-psoriatic herbal candidate; however, the molecular basis of its bioactive metabolites remains insufficiently understood. This study investigated the anti-psoriatic potential of cucurbitane-type triterpenoids from *M. charantia* using integrated network pharmacology and molecular docking. Of 192 secondary metabolites, 50 passed pharmacokinetic and toxicity screening, yielding 347 predicted human targets, of which 159 overlapped with 3,383 psoriasis-associated genes. Key hub genes identified by protein-protein interaction and topological analyses included AKT1, TNF, EGFR, STAT3, IL1B, CASP3, MMP9, HIF1A, and ESR1, with enriched biological processes related to oxidative stress, lipid and hormonal responses, and intracellular receptor signaling. Molecular docking of five cucurbitane-type triterpenoids against four validated hub proteins demonstrated consistently favorable predicted binding affinities for AKT1 via its allosteric pocket, as well as for EGFR and IL1B. Karavilagenin A showed the most favorable binding energy against AKT1, momordicin I against EGFR and IL1B, and cucurbitacin B demonstrated favorable profiles across multiple targets. These findings suggest that *M. charantia* may influence psoriasis-related biology through multi-target mechanisms, providing a basis for further experimental validation.

Keywords: cucurbitane-type triterpenoids; *Momordica charantia*; molecular docking; network pharmacology; psoriasis

Introduction

Psoriasis is a chronic immune-mediated inflammatory disease characterized by excessive keratinocyte proliferation, persistent inflammation, and the formation of erythematous scaly plaques on the skin [1]. This disease not only causes physical discomfort but also significantly impairs patients' quality of life due to its recurrent nature and the need for long-term treatment. Globally, psoriasis is estimated to affect approximately 2–3% of the population, or nearly 125 million people [2]. The reported prevalence varies considerably across populations, ranging from 0.51% to 11.43% in adults and from 0% to 1.37% in children, demonstrating substantial geographical and age-related variation in its epidemiological distribution [3]. Together with its considerable global disease burden, these variations reinforce the importance of psoriasis as a major public health concern [4].

The pathogenesis of psoriasis involves complex interactions among immune cells, inflammatory mediators, and proteins regulating cell proliferation and survival [5,6]. Key molecular players include tumor necrosis factor (TNF) and interleukin-1 beta (IL-1B), which amplify inflammatory cascades; epidermal growth factor receptor (EGFR) and signal transducer and activator of transcription 3 (STAT3), which regulate keratinocyte proliferation and survival; caspase-3 (CASP3), which participates in apoptosis regulation; and hypoxia-inducible factor 1-alpha (HIF1A) together with matrix metalloproteinases (MMP9, MMP2), which are associated with microenvironmental adaptation and tissue remodeling [5,6,7,8]. The involvement of prostaglandin-endoperoxide synthase 2 (PTGS2) and estrogen receptor 1 (ESR1) further reflects the contribution of lipid mediator pathways and hormonal-immune interactions to psoriatic pathology [9,10]. Accordingly, therapeutic

Copyright © The Author(s) 2026. This article is distributed under a Creative Commons Attribution 4.0 International License

approaches to psoriasis are no longer viewed solely from a single-target perspective but rather through the involvement of multiple interconnected biological targets within a disease network. This complexity has sustained interest in the search for novel therapeutic candidates, including those derived from natural products, in which multiple bioactive constituents may exert therapeutic effects through multi-target and multi-pathway mechanisms [11].

One plant of particular interest is *Momordica charantia* L., commonly known as bitter melon. This plant has long been used in traditional medicine and is recognized for its diverse biological activities, including anti-inflammatory, antioxidant, antidiabetic, and immunomodulatory effects [12,13]. Among its secondary metabolites, cucurbitane-type triterpenoids represent the chemotaxonomically distinctive class of compounds characteristic of *M. charantia* and the broader Cucurbitaceae family, differentiating them from widely distributed phytochemicals such as flavonoids and phytosterols that have been extensively investigated in other plant systems [12,13]. In addition to its widespread use as an herbal remedy, preclinical evidence has shown that the ethanolic leaf extract of *M. charantia* exhibits anti-psoriatic activity in a mouse-tail model, as indicated by an increase in the degree of orthokeratosis of approximately 64% [14]. Furthermore, cucurbitacin B, a cucurbitane-type triterpenoid from this plant, has been experimentally demonstrated to attenuate psoriatic skin lesions and reduce serum levels of IL-6, TNF-alpha, and IL-1beta in an imiquimod-induced mouse model, with a proposed mechanism involving downregulation of the cGAS-STING signaling pathway [15]. These findings collectively suggest that bitter melon and its cucurbitane-type triterpenoids may serve as a promising source of active compounds for psoriasis management, although the molecular mechanisms underlying the activity of these metabolites remain insufficiently understood.

Network pharmacology provides a systems-level analytical framework for investigating the relationships among natural compounds, molecular targets, biological pathways, and disease-associated genes. In contrast to the conventional one-drug-one-target paradigm, this approach enables the construction and analysis of multi-component, multi-target, and multi-pathway interaction networks. It is particularly relevant to medicinal plant research because a single plant may contain numerous secondary metabolites that can interact with different but interconnected biological targets and collectively modulate disease-related processes. Accordingly, network pharmacology has been increasingly applied to identify active phytochemicals, predict their potential targets, characterize protein-protein interaction networks, and elucidate the biological pathways underlying the pharmacological effects of medicinal plants [11,16].

Molecular docking was employed alongside network pharmacology to provide complementary structural information by predicting plausible ligand-binding poses, estimated binding affinities, and non-covalent interactions within the binding sites of target proteins. The integration of these two approaches has been increasingly applied to prioritize natural compounds and assess whether predicted network targets are structurally compatible with selected ligands [17,18,19]. Among the screened metabolites, five cucurbitane-type triterpenoids, namely cucurbitacin B, karavilagenin A, karavilagenin B, karaviloside II, and momordicin I, were selected for molecular docking based on three considerations: their representation of the chemotaxonomically distinctive cucurbitane scaffold of *M. charantia*; the experimental evidence supporting the anti-psoriatic relevance of this compound class, particularly cucurbitacin B [15]; and the structural diversity they collectively represent within the cucurbitane series, including oxygenated cucurbitacins, ring-modified variants, a glycosidic form, and an aldehyde-substituted derivative, enabling a preliminary computational exploration of structure-related binding differences within a chemically coherent ligand series. The docking results were therefore interpreted as computational support for the predicted compound-target associations identified through network pharmacology rather than as definitive evidence of binding affinity or biological activity, thereby strengthening the rationale for further experimental investigation of the anti-psoriatic potential of characteristic *M. charantia* metabolites [20].

Based on this background, the present study was conducted to provide a clearer understanding of the relationship between the secondary metabolites of *M. charantia* and protein targets associated with psoriasis through integrated network pharmacology and molecular docking approaches. Specifically, this study aimed to: (i) identify metabolites that meet in silico pharmacokinetic and toxicity screening criteria; (ii) predict the protein targets of screened metabolites and determine their overlap with psoriasis-associated genes; (iii) analyze the dominant protein-protein interaction network and biological processes associated with the overlapping targets; and (iv) evaluate selected

cucurbitane-type triterpenoids through molecular docking against hub proteins to estimate their binding affinities and ligand-protein interaction patterns. The findings of this study are expected to provide a scientific basis for understanding the potential of *M. charantia* as an anti-psoriatic herbal candidate and a preliminary foundation for further computational and experimental validation studies.

Methods

Identification of secondary metabolites of *M. charantia*

Secondary metabolite data of *M. charantia* were retrieved from KNApSAcK (https://www.knapsackfamily.com/) and Dr. Duke's Phytochemical and Ethnobotanical Databases (https://phytochem.nal.usda.gov/). The chemical structures of the identified compounds, in the form of canonical SMILES, were subsequently obtained from PubChem (https://pubchem.ncbi.nlm.nih.gov/) [21]. The retrieved data were curated and deduplicated in Microsoft Excel for further analysis [18,22].

Screening of secondary metabolites

Compound screening was performed in three sequential steps to identify metabolites with favorable druglikeness, adequate predicted bioavailability, and low predicted toxicity. First, drug-likeness was assessed using MolSoft (https://molsoft.com/mprop/). A threshold of ≥0.10 was applied to exclude compounds with zero or negative scores, which are statistically more similar to non-drug molecules, while retaining natural product scaffolds that may deviate from conventional drug-like space but still demonstrate a positive drug-likeness estimate. This inclusive initial cutoff is consistent with the multilayered screening approach employed in network pharmacology studies of plant-derived compounds, where subsequent pharmacokinetic and toxicity filters serve as progressively stringent selection steps [23,24].

Second, compounds passing the drug-likeness threshold were evaluated using SwissADME (http://www.swissadme.ch/) for compliance with Lipinski's Rule of Five and the bioavailability score [25]. A tolerance of fewer than two Lipinski violations was applied, acknowledging that naturally occurring secondary metabolites, particularly terpenoids and steroids, may deviate marginally from one conventional oral drug-likeness parameter while retaining acceptable bioavailability profiles [23,24]. A bioavailability score of ≥0.55 was required, as this represents the minimum acceptable score within the SwissADME scoring system for compounds satisfying basic pharmacokinetic requirements across the evaluated property parameters, whereas a score of 0.17 indicates multiple pharmacokinetic liabilities [25].

Third, predicted toxicity was evaluated using ADMETlab 3.0 (https://admetlab3.scbdd.com/) [26]. A predicted probability threshold of <0.70 was applied for both hERG channel blockade at 10 μM and Ames mutagenicity, classifying compounds below this cutoff as unlikely to exhibit these toxic properties based on the platform's machine learning prediction models. This threshold reflects the boundary commonly applied in computational ADMET studies to distinguish compounds with acceptable predicted safety profiles from those flagged as probable toxicants [23,26]. Compounds fulfilling all three sequential screening steps were retained for further analysis.

Prediction of target genes of *M. charantia* metabolites

Protein target prediction for the screened compounds was performed using two complementary platforms: TargetNet (http://targetnet.scbdd.com/) and the Similarity Ensemble Approach (SEA; https://sea.bkslab.org/), with the analysis restricted to human targets (*Homo sapiens*). The results from both platforms were combined, and duplicate targets were removed and standardized to official human gene symbols, yielding the final list of predicted target genes associated with the screened metabolites of *M. charantia* [18,22].

Prediction of psoriasis-related genes

Psoriasis-related genes were retrieved from GeneCards (https://www.genecards.org/) using "psoriasis" as the search keyword. The identified genes were compiled, deduplicated, and standardized to official human gene symbols to obtain the final list of psoriasis-associated targets for subsequent overlap analysis [18,22].

Construction of Venn diagram and identification of overlapping targets

The predicted target genes of *M. charantia* metabolites and psoriasis-related genes were compared using Venny (https://bioinfogp.cnb.csic.es/tools/venny/) to identify overlapping targets. These overlapping genes were considered potential therapeutic targets of *M. charantia* against psoriasis and were used for subsequent network and enrichment analyses [18,22].

Protein-protein interaction network analysis and hub gene identification

The overlapping targets were analyzed using STRING-DB (https://string-db.org/) with the organism set to *Homo sapiens* and a minimum interaction confidence score of ≥0.7 to construct a protein-protein interaction (PPI) network. The resulting network was further analyzed in Cytoscape (https://cytoscape.org/) using the CytoHubba plugin (http://apps.cytoscape.org/apps/cytohubba) to identify hub genes based on two topological parameters: degree, which measures the number of direct interaction partners of each node, and Maximal Clique Centrality (MCC), which emphasizes participation in densely interconnected subnetworks. The top 10 hub genes identified by each parameter were reported and compared [18,22].

Gene ontology enrichment analysis

Gene Ontology (GO) enrichment analysis was performed using STRING-DB to identify dominant biological processes associated with the overlapping targets, with emphasis on the Biological Process (BP) category. The enrichment results were evaluated based on false discovery rate (FDR) values, and the significantly enriched biological processes were interpreted to characterize the potential mechanisms through which *M. charantia* metabolites may influence psoriasis-related biology [18,22].

Selection of target proteins and ligands

Based on the network pharmacology results, five hub proteins were initially considered for molecular docking: EGFR, STAT3, IL1B, PTGS2, and AKT1. However, preliminary docking trials against PTGS2 produced markedly anomalous binding energy values for all tested ligands, including strongly positive scores that are physically implausible and indicative of technical artifacts rather than true ligand-receptor incompatibility. Potential sources of error include protonation state inconsistencies in ligand preparation, charge-assignment artifacts, or incompatibility between the cucurbitane triterpenoid scaffold and the geometric constraints of the evaluated binding pocket. Because corrective measures, including the use of alternative protein structures, alternative binding site definitions, or alternative docking parameters, could not be adequately implemented within the scope of this study, PTGS2 was excluded from the docking analysis. Its relevance to psoriasis biology and its position as a network hub gene, however, remain supported by the network pharmacology findings and existing pharmacological literature. Accordingly, molecular docking was performed for four target proteins: EGFR, STAT3, IL1B, and AKT1.

The three-dimensional structures of the four target proteins were retrieved from the RCSB Protein Data Bank [27]. The selection of each structure was based on the availability of a co-crystallized small-molecule ligand that defined the binding site, structural resolution, and relevance of the binding pocket to the known pharmacology of each target. EGFR was represented by PDB 1M17, which contains a 4-anilinoquinazoline inhibitor occupying the ATP-binding site of the kinase domain [28]. STAT3 was represented by PDB 6NUQ, which contains the small-molecule inhibitor SI-109 bound to the SH2 domain, a pharmacologically relevant interface for STAT3 dimerization and transcriptional activation [29]. IL1B was represented by PDB 8C3U, a high-resolution structure containing a peptide-based inhibitor (T9C) that defines the binding interface of IL-1beta. For AKT1, PDB 3O96 was selected because it contains AKT Inhibitor VIII, an allosteric inhibitor that occupies the interface between the pleckstrin homology (PH) domain and the kinase domain, locking AKT1 in an inactive closed conformation [30]. The grid box for AKT1 docking was therefore defined around this allosteric binding pocket rather than the ATP-binding site. Allosteric inhibition of AKT1 through the PH domain-kinase domain interface represents a mechanistically distinct mode of inhibition compared with ATP-competitive binding, and the binding energy values reported for AKT1 in this study represent predicted affinities toward this allosteric pocket [31].

Five cucurbitane-type triterpenoids from *M. charantia*, namely cucurbitacin B, karavilagenin A, karavilagenin B, karaviloside II, and momordicin I, were selected as test compounds. Their two-dimensional structures were obtained from PubChem [21] and converted into three-dimensional models using Avogadro [32], followed by geometry optimization using the PM6 semi-empirical method [33] in Gaussian 16 through the GaussView interface [34].

Docking protocol and validation

Molecular docking was performed using AutoDock 4.2, with AutoDockTools 1.5.4 used for molecular preparation and docking setup [35]. Protein preparation involved the removal of water molecules and co-crystallized ligands, addition of polar hydrogen atoms, and assignment of Kollman charges. Ligands were

prepared by assigning Gasteiger charges and defining rotatable bonds. For each target protein, the grid box was centered on the binding site defined by the coordinates of the corresponding co-crystallized ligand to restrict the conformational search to the native binding pocket. Docking simulations were conducted using the Lamarckian Genetic Algorithm with default parameters.

The docking protocol was validated by redocking each co-crystallized ligand into its original binding pocket. The resulting poses were evaluated using root mean square deviation (RMSD) values calculated between the redocked pose and the experimentally observed ligand conformation. An RMSD value below 2.0 Å was used as the criterion for acceptable protocol reproduction, consistent with the standard threshold applied in computational docking validation studies [20,35]. The best-ranked conformations of the test compounds were selected based on the lowest predicted binding energy and their clustering profiles.

Interaction analysis

Ligand-protein interactions within the binding sites were visualized and analyzed using BIOVIA Discovery Studio Visualizer. The analysis encompassed hydrogen bonds, hydrophobic contacts, and other non-covalent interactions between the ligands and amino acid residues within the binding pocket. The interaction patterns of the test compounds were subsequently compared with those of the corresponding co-crystallized ligands to assess similarities in binding-site occupation and residue involvement.

Results

Identification and screening of secondary metabolites of *M. charantia*

A total of 192 secondary metabolites of *M. charantia* were identified from the KNApSAcK and Dr. Duke's Phytochemical and Ethnobotanical Databases. The chemical structures of these compounds were standardized using canonical SMILES obtained from PubChem [21]. The compounds were subsequently subjected to stepwise screening using MolSoft, SwissADME [25], and ADMETlab 3.0 [26] based on drug-likeness score, compliance with Lipinski's Rule of Five, bioavailability score, and predicted toxicity. Of 192 metabolites, 122 were excluded at the drug-likeness and pharmacokinetic screening steps, and a further 20 were excluded based on predicted hERG blockade or Ames mutagenicity, yielding 50 metabolites that fulfilled all in silico screening criteria and were retained for further analysis. The screened metabolites are presented in Table 1.

Prediction of target genes of *M. charantia* metabolites and psoriasis-related genes

The 50 screened metabolites were analyzed using TargetNet and SEA to predict their potential human protein targets. After removal of duplicates and standardization to official human gene symbols, 347 unique metabolite-related targets were obtained. In parallel, psoriasis-associated genes were retrieved from GeneCards using "psoriasis" as the search term, yielding 3,383 unique psoriasis-associated genes.

Identification of overlapping targets

The predicted human targets of the screened *M. charantia* metabolites were compared with psoriasis-associated genes using a Venn diagram. A total of 159 overlapping genes were identified between the 347 predicted metabolite-related targets and the 3,383 psoriasis-associated genes, with the non-overlapping regions comprising 188 metabolite-related targets and 3,224 psoriasis-related genes. These 159 overlapping genes were considered putative targets through which *M. charantia* metabolites may influence psoriasis-related biological processes and were used for subsequent protein-protein interaction and enrichment analyses. The overlap analysis is presented in Figure 1.

Protein-protein interaction network analysis and hub gene identification

The 159 overlapping genes were imported into STRING-DB for PPI analysis using the *Homo sapiens* setting and a confidence score of ≥0.7. The resulting PPI network was further analyzed in Cytoscape using the CytoHubba plugin to rank hub genes based on degree and MCC. Based on degree, the top 10 hub genes were TNF, AKT1, EGFR, IL1B, STAT3, CASP3, PTGS2, MMP9, HIF1A, and ESR1, with TNF showing the highest degree value (85), followed by AKT1 (84) and EGFR (78). Based on MCC, the top 10 hub genes were AKT1, TNF, HIF1A, STAT3, EGFR, MMP9, PTGS2, CASP3, ESR1, and MMP2. Several genes, including AKT1, TNF, EGFR, STAT3, PTGS2, MMP9, CASP3, and ESR1, appeared in both rankings, supporting their structural importance within the constructed network. The PPI network and hub gene analyses are presented in Figures 2 and 3, and the comparative ranking is summarized in Table 2.

Table 1. Secondary metabolites of *Momordica charantia* that passed stepwise in silico screening for drug-likeness, bioavailability, and predicted toxicity (n = 50).

Secondary Metabolite	Druglikeness	Bioavailability Score	Violation of Lipinski
Requirement	**≥0.10**	**≥0.55**	**<2**
3,4-Dihydroxybenzoic acid	0.23	0.56	0
Gentisic acid	0.30	0.56	0
Resorcylic acid	0.32	0.56	0
3-Hydroxyflavone	0.12	0.55	0
Naringenin chalcone	0.23	0.55	0
Biochanin A	0.15	0.55	0
Kaempferol	0.50	0.55	0
(+)-Dihydrokaempferol	0.85	0.55	0
(-)-Epicatechin	0.64	0.55	0
(+)-Catechin	0.64	0.55	0
Quercetin	0.52	0.55	0
Dihydroquercetin	1.00	0.55	0
20,21,22,23,24,25,26,27-Octanorcucurbit-5-ene-3,7,17-trione	0.46	0.55	0
23,24,25,26,27-Pentanor-3,7-dioxocucurbit-5-en-22-oic acid	0.68	0.85	0
Kuguacin L	0.12	0.55	0
3beta-Hydroxy-(22E,24R)-ergosta-5,8,22-trien-7-one	0.68	0.55	1
beta-Stigmasterol	0.62	0.55	1
Clerosterol	0.68	0.55	1
Kuguacin C	0.52	0.55	1
(-)-beta-Sitosterol	0.78	0.55	1
Momordenol	0.96	0.55	1
beta-Amyrin	0.22	0.55	1
Cucurbitadienol	0.38	0.55	1
Kuguacin D	0.47	0.55	1
Kuguacin K	0.13	0.56	0
Cucurbita-5,23,25-triene-3,7-dione	0.28	0.55	1
13beta,28-Epoxy-11-ursen-3-one	0.35	0.55	1
Cucurbita-5,24-diene-3,7,23-trione	0.53	0.55	1
7-Methoxycucurbita-5,23,25-trien-3-ol	0.12	0.55	1
Kuguacin B	0.68	0.55	0
Kuguacin O	0.44	0.55	0
Kuguacin S	0.62	0.55	0
(23E)-3beta-Hydroxy-7beta-methoxycucurbita-5,23,25-trien-19-al	0.12	0.55	1
Kuguacin A	0.59	0.55	1
Kuguacin N	0.19	0.55	0
Momordicin	0.68	0.55	1

Secondary Metabolite	Druglikeness	Bioavailability Score	Violation of Lipinski
Requirement	**≥0.10**	**≥0.55**	**<2**
(3S,7S,8S,9R,10R,13R,14S,17R)-3,7-Dihydroxy-17-[(E,2R)-6-hydroxy-6-methylhept-4-en-2-yl]-4,4,13,14-tetramethyl-2,3,7,8,10,11,12,15,16,17-decahydro-1H-cyclopenta[a] phenanthrene-9-carbaldehyde	0.24	0.55	0
Momordicin I	0.33	0.55	0
Karavilagenin B	0.31	0.55	1
Karavilagenin C	0.41	0.55	1
Kuguacin H	0.56	0.55	0
3,7-Dihydroxy-25-methoxycucurbita-5,23-dien-19-al	0.21	0.55	1
Karavilagenin A	0.26	0.55	1
Kuguacin I	0.11	0.55	0
Cucurbitacin F	0.36	0.55	1
beta-Carotene	0.64	0.85	0
beta-Cryptoxanthin	0.78	0.85	0
Cucurbitacin B	0.13	0.55	1
Karaviloside III	0.25	0.55	1
Karaviloside II	0.20	0.55	1

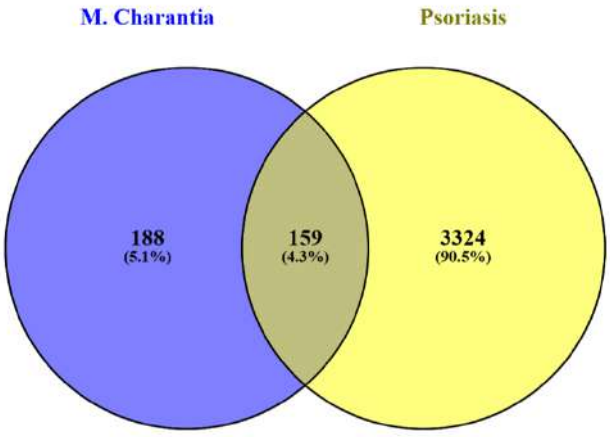


Figure 1. Venn diagram of overlapping genes between *Momordica charantia* metabolite-predicted targets and psoriasis-associated genes. A total of 159 overlapping genes were identified between 347 predicted human targets of *M. charantia* metabolites and 3,383 psoriasis-associated genes retrieved from GeneCards. Non-overlapping regions comprise 188 metabolite-related targets and 3,224 psoriasis-related genes.

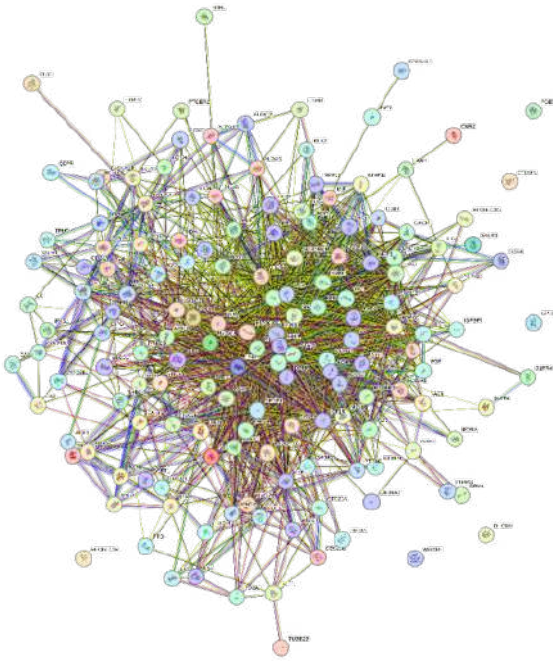


Figure 2. Protein-protein interaction (PPI) network of 159 overlapping genes between *Momordica charantia* metabolite-predicted targets and psoriasis-associated genes. The network was constructed using STRING-DB with *Homo sapiens* as the reference organism and a minimum confidence score of ≥0.7. Each node represents a protein and each edge represents a predicted functional interaction.

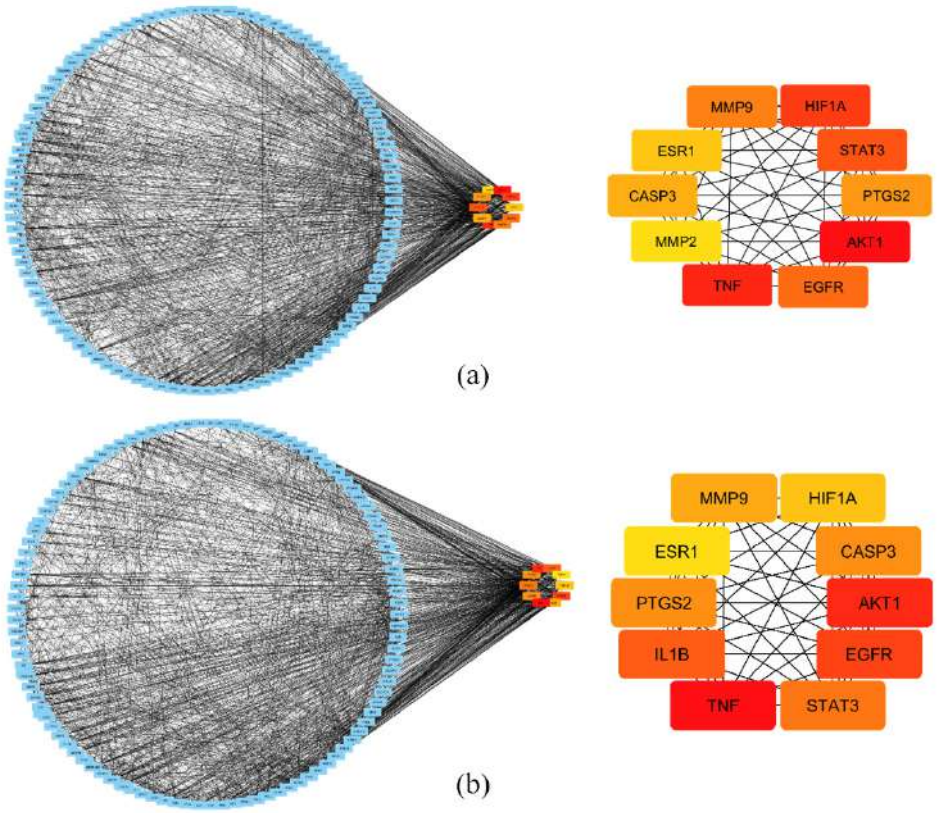


Figure 3. Top 10 hub genes identified from the PPI network based on (a) Maximal Clique Centrality (MCC) and (b) degree. Hub genes were ranked using the CytoHubba plugin in Cytoscape. Node color intensity reflects the ranking score, with darker nodes indicating higher centrality values.

Table 2. Comparison analysis of 10 hub genes based on degree and maximal clique centrality (MCC)

Rank	Gen	Degree	Gen	MCC Log Score
1	TNF	85	AKT1	19.11921
2	AKT1	84	TNF	19.11921
3	EGFR	78	HIF1A	19.11921
4	IL1B	74	STAT3	19.11921
5	STAT3	72	EGFR	19.11909
6	CASP3	68	MMP9	19.11894
7	PTGS2	68	PTGS2	19.11892
8	MMP9	67	CASP3	19.11891
9	HIF1A	66	ESR1	19.11889
10	ESR1	65	MMP2	19.11822

Gene ontology enrichment analysis

Gene Ontology enrichment analysis of the 159 overlapping genes identified several dominant biological processes, including response to amyloid-beta, response to oxygen-containing compound, response to lipid, response to hormone, cellular response to lipid, response to peptide, cellular response to oxygen-containing compound, cellular response to hormone stimulus, response to xenobiotic stimulus, and intracellular receptor signaling pathway. All reported terms reached

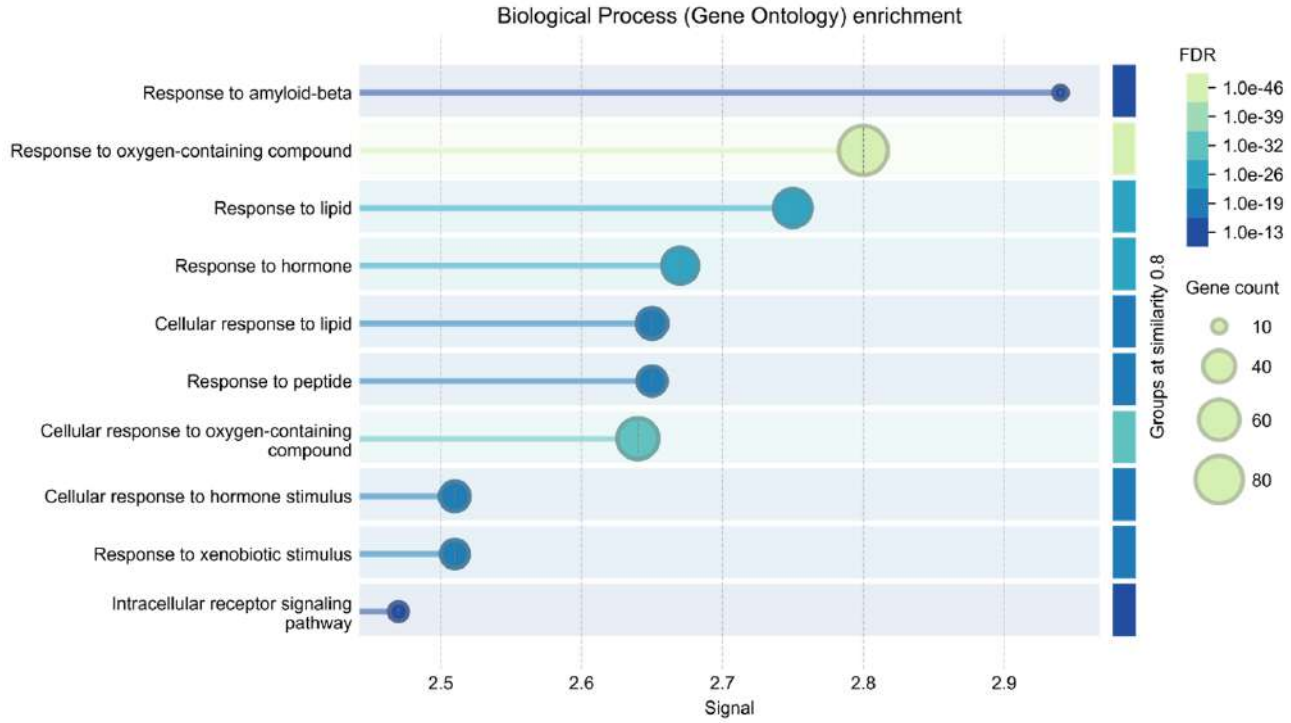


Fig 4. Gene Ontology Biological Process (GO-BP) enrichment bubble plot of 159 overlapping genes between *Momordica charantia* metabolite-predicted targets and psoriasis-associated genes. The horizontal axis represents enrichment strength, bubble size represents the number of genes associated with each term, and color gradient indicates statistical significance based on false discovery rate (FDR).

statistical significance based on false discovery rate (FDR) values. In the enrichment bubble plot, the horizontal axis represents enrichment strength, bubble size represents gene count, and color indicates the significance level based on FDR. The GO-BP enrichment results are shown in Figure 4.

Molecular docking analysis

Docking protocol validation

Docking protocol validation was performed by redocking the co-crystallized ligands into the original binding pockets of the four selected target proteins. All protein-ligand complexes yielded RMSD values below the 2.0 Å threshold: EGFR-4-anilinoquinazoline (1M17, 1.71 Å), STAT3-SI-109 (6NUQ, 1.12 Å), IL1B-T9C (8C3U, 0.62 Å), and AKT1-AKT Inhibitor VIII (3O96, 1.10 Å), confirming that the docking protocol was capable of reproducing the experimentally observed binding poses within the predefined binding sites. The docking validation results are summarized in Table 3.

Binding energy of cucurbitane-type triterpenoids

Docking of the five selected cucurbitane-type triterpenoids against the four validated target proteins showed variable binding affinities. For EGFR (1M17), the most favorable binding energy was observed for momordicin I (-8.86 kcal/mol), followed by karavilagenin A (-8.52 kcal/mol) and karavilagenin B (-8.16 kcal/mol). For STAT3 (6NUQ), cucurbitacin B produced the most favorable binding energy (-7.02 kcal/mol), followed by karavilagenin B (-6.82 kcal/mol) and momordicin I (-6.68 kcal/mol). For IL1B (8C3U), momordicin I showed the most favorable binding energy (-8.36 kcal/mol), followed by cucurbitacin B (-7.61 kcal/mol) and karavilagenin B (-7.57 kcal/mol). For AKT1 (3O96), all five ligands produced comparatively favorable binding energies, with karavilagenin A showing the most favorable value (-10.86 kcal/mol), followed by cucurbitacin B (-10.60 kcal/mol) and momordicin I (-10.51 kcal/mol). Overall, AKT1 yielded the most consistently favorable binding energies across all tested ligands, followed by EGFR and IL1B. The predicted binding energies are summarized in Table 4.

Table 3. Docking validation results showing grid box parameters, binding site coordinates, RMSD values, and binding energies of co-crystallized ligands redocked into their original binding pockets.

PDB ID	Gridbox			Coordinates			RMSD	Binding energy
	x	y	z	x	y	z		
1M17-EGFR (4-anilinoquinazoline)	44	24	24	21.697	0.303	52.093	1.71	-8.01
6NUQ-STAT3 (SI-109)	40	56	40	13.619	54.024	-0.083	1.12	-10.17
8C3U-IL1B (T9C)	30	30	26	-16.845	5.696	-42.888	0.62	-11.92
5IKR-PTGS2 (Mefenamic Acid)	28	22	24	38.042	2.131	61.279	0.56	-7.6
3O96-AKT1 (AKT inhibitor VIII)	30	44	40	9.657	-7.761	10.604	1.1	-12.89

Table 4. Predicted binding energies (kcal/mol) of five cucurbitane-type triterpenoids from *Momordica charantia* against four psoriasis-associated target proteins. More negative values indicate more favorable predicted binding.

Protein (PDB ID)	Cucurbitacin B	Karavilagenin A	Karavilagenin B	Karaviloside II	Momordicin I
EGFR (1M17)	-7.7	-8.52	-8.16	-7.28	-8.86
STAT3 (6NUQ)	-7.02	-6.62	-6.82	-5.73	-6.68
IL1B (8C3U)	-7.61	-6.94	-7.57	-3.03	-8.36
AKT1 (3O96)	-10.6	-10.86	-10.36	-9.3	-10.51

Ligand-protein interaction analysis

Analysis of ligand-protein interactions using BIOVIA Discovery Studio Visualizer identified hydrogen bonds, hydrophobic contacts, and other non-covalent interactions between each cucurbitane-type triterpenoid and the amino acid residues within the binding pockets of EGFR, STAT3, IL1B, and AKT1. The interaction profiles of the test compounds were compared with those of the corresponding co-crystallized ligands to assess similarities in binding-site occupation and residue involvement. The identified interactions for each protein-ligand pair are summarized in Tables 5–8. Representative two-dimensional interaction diagrams for selected protein-ligand complexes are shown in Figures 5–8.

Table 5. Predicted ligand-protein interactions of cucurbitane-type triterpenoids with EGFR (PDB: 1M17). Interactions of the co-crystallized ligand (4-anilinoquinazoline) are included for comparison.

Ligand	Hydrogen bond residues	Hydrophobic contact residues	Other interactions
4-anilinoquinazoline (reference)	Met769, Cys773, Gly772, Gln767, Asp776, Pro770	Leu820, Lys721, Met742, Leu764, Ala719, Leu694	-
Cucurbitacin B	Pro770	Lys721, Met742	-
Karavilagenin A	Lys721, Asp831, Gln767	Leu694, Val702, Leu820, Lys721	-
Karavilagenin B	Lys721, Asp831	Leu694, Val702, Leu820, Cys773, Lys721, Met769	-
Karaviloside II	Thr766, Glu738	Val702, Cys773, Leu820	-
Momordicin I	Met769, Ala719, Leu764, Leu694, Thr766	Leu694, Val702, Ala719, Leu820, Leu768, Lys721, Met742	-

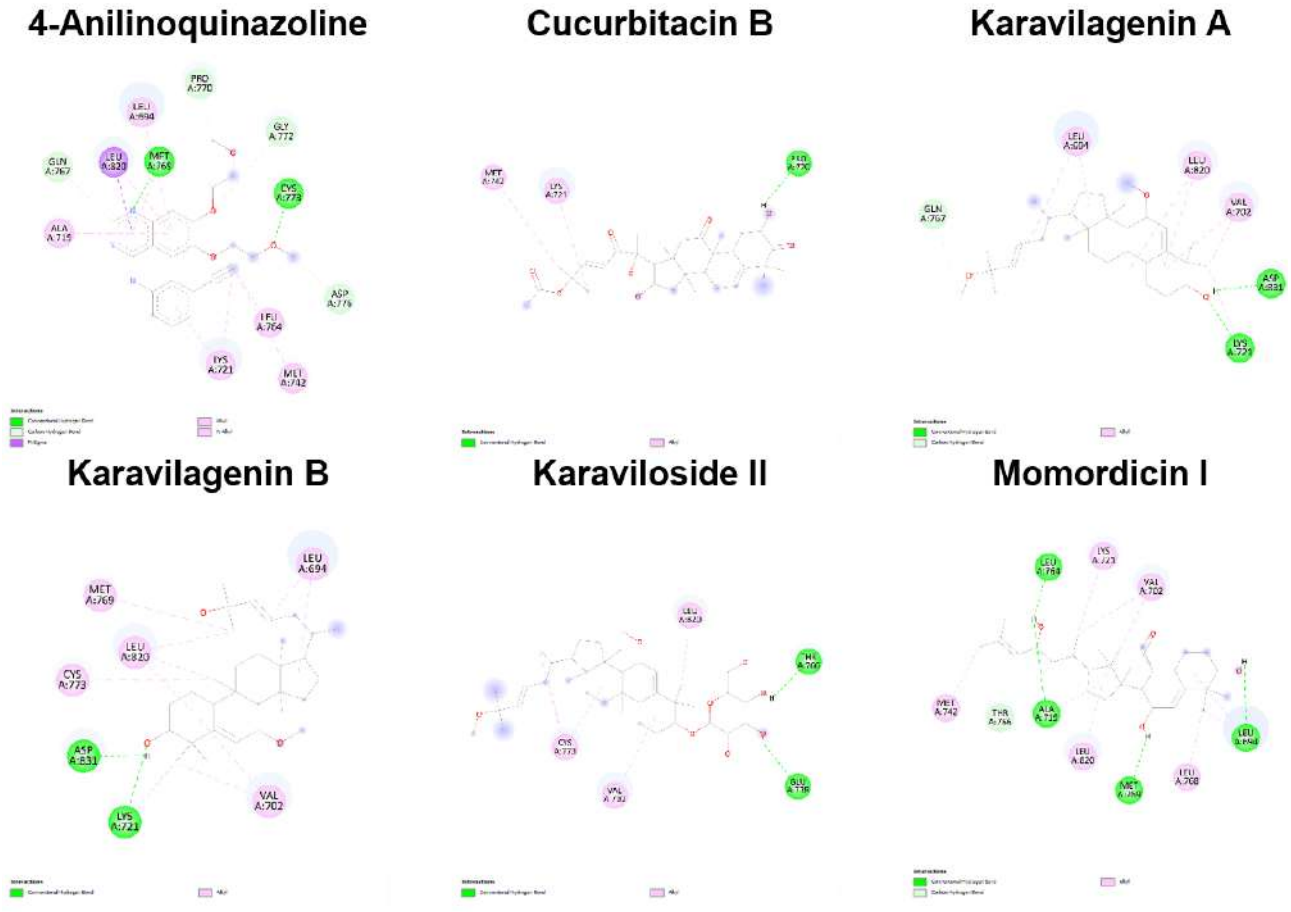


Fig 5. Ligand-protein interaction diagrams of cucurbitane-type triterpenoids within the binding site of EGFR (PDB: 1M17). Two-dimensional interaction diagrams were generated using BIOVIA Discovery Studio Visualizer. The co-crystallized ligand 4-anilinoquinazoline is shown for comparison. Hydrogen bonds are indicated by green dashed lines, hydrophobic contacts by pink arcs, and other non-covalent interactions as labeled.

Table 6. Predicted ligand-protein interactions of cucurbitane-type triterpenoids with STAT3 (PDB: 6NUQ). Interactions of the co-crystallized ligand (SI-109) are included for comparison.

Ligand	Hydrogen bond residues	Hydrophobic contact residues	Other interactions
SI-109 (reference)	Ser613, Glu638, Tyr640, Gln644, Tyr657, Ser636	Tyr657, Pro639	Arg609, Lys658
Cucurbitacin B	Tyr640, Gln644, Lys658, Ser636	-	-
Karavilagenin A	Glu638, Lys658	Tyr640, Val637, Lys658, Tyr657	-
Karavilagenin B	Glu638, Lys658	Tyr640, Val637, Lys658, Tyr657	-
Karaviloside II	Glu638, Gln644	Tyr640, Val637, Lys658, Tyr657, Ile659, Met660, Leu666	-
Momordicin I	Gln644, Ser636	Val637, Trp623	-

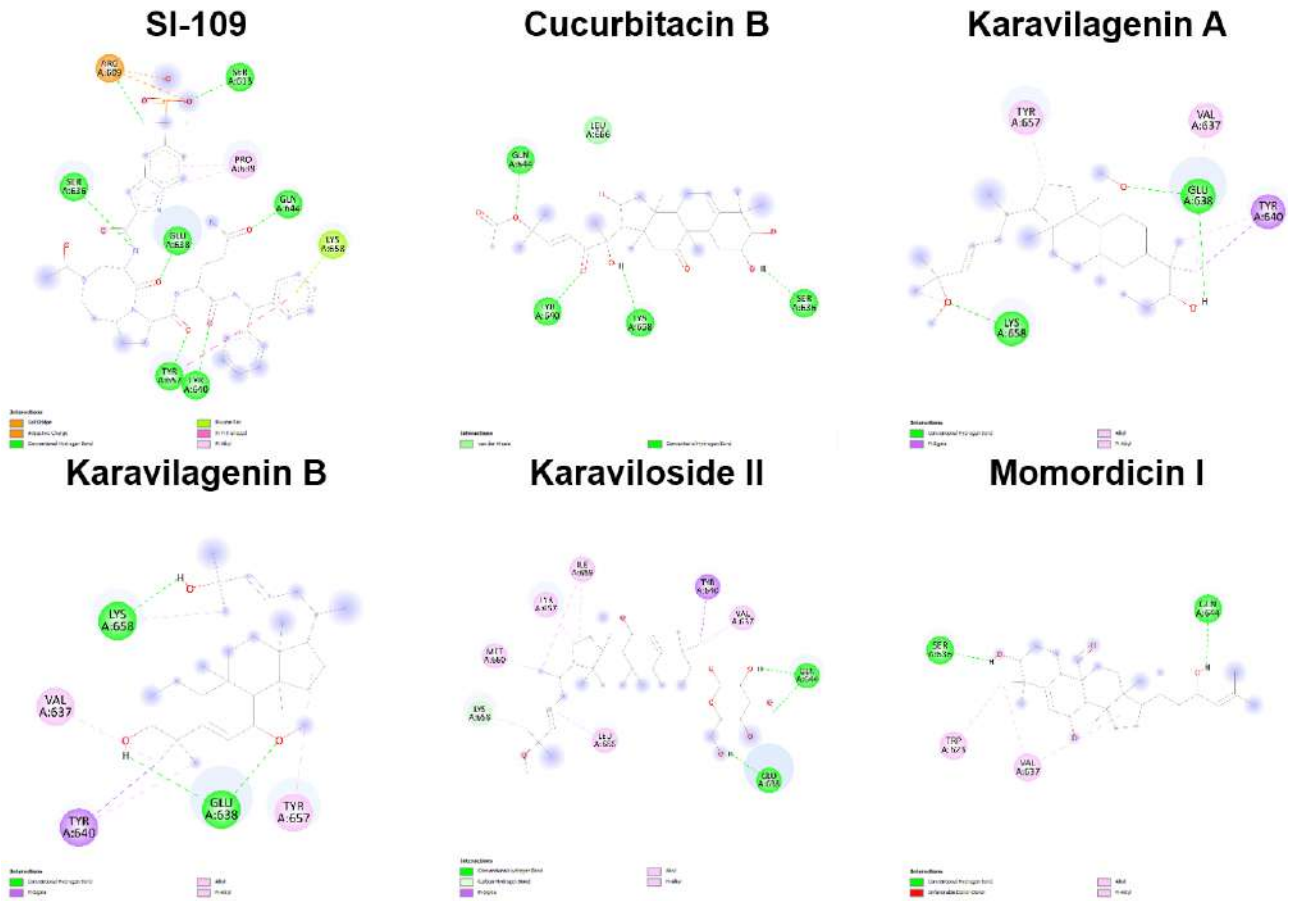


Fig 6. Ligand-protein interaction diagrams of cucurbitane-type triterpenoids within the binding site of STAT3 (PDB: 6NUQ). Two-dimensional interaction diagrams were generated using BIOVIA Discovery Studio Visualizer. The co-crystallized ligand SI-109 is shown for comparison. Hydrogen bonds are indicated by green dashed lines, hydrophobic contacts by pink arcs, and other non-covalent interactions as labeled.

Table 7. Predicted ligand-protein interactions of cucurbitane-type triterpenoids with IL1B (PDB: 8C3U). Interactions of the co-crystallized ligand (T9C) are included for comparison.

Ligand	Hydrogen bond residues	Hydrophobic contact residues	Other interactions
T9C (reference)	Lys94, Met95, Lys97, Asn102, Lys93, Glu50	Val47, Val100, Ala115, Ala59, Val3, Pro91, Met95, Pro57	Lys94
Cucurbitacin B	Asn102, Pro57, Phe46	Lys94	-
Karavilagenin A	Asn102, Lys94, Ser45	Val47, Pro57, Ala59, Lys97, Val100, Ala115, Met95	-
Karavilagenin B	Asn53, Lys94, Lys93, Lys55	Lys55, Pro57, Ala115, Val100, Met95	-
Karaviloside II	Pro57, Met95, Lys94	Pro57, Val100, Ala115	-
Momordicin I	Lys93, Asn102, Pro57	Val47, Pro57, Ala59, Lys97, Val100, Ala115, Val3, Met95	-

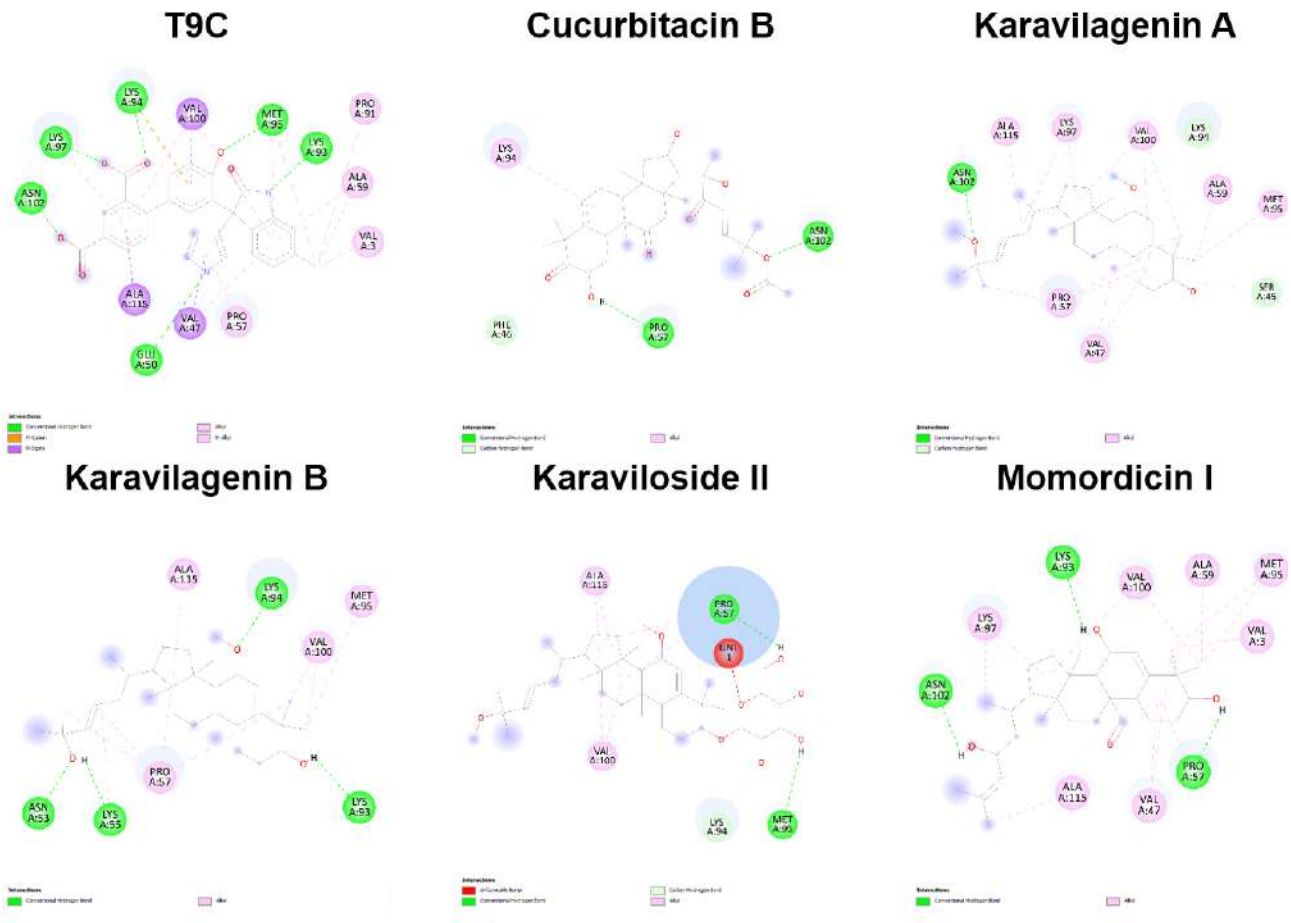


Fig 7. Ligand-protein interaction diagrams of cucurbitane-type triterpenoids within the binding site of IL1B (PDB: 8C3U). Two-dimensional interaction diagrams were generated using BIOVIA Discovery Studio Visualizer. The co-crystallized ligand T9C is shown for comparison. Hydrogen bonds are indicated by green dashed lines, hydrophobic contacts by pink arcs, and other non-covalent interactions as labeled.

Table 8. Predicted ligand-protein interactions of cucurbitane-type triterpenoids with the allosteric binding pocket of AKT1 (PDB: 3O96). Interactions of the co-crystallized ligand (AKT Inhibitor VIII) are included for comparison.

Ligand	Hydrogen bond residues	Hydrophobic contact residues	Other interactions
AKT Inhibitor VIII (reference)	Asn54	Ile84, Trp80, Arg273, Leu264, Lys268, Val270, Leu210	Arg273, Asp292, Lys268, Tyr326
Cucurbitacin B	Gln79, Tyr272	Gln79, Trp80, Ile84, Leu210, Tyr263, Leu264, Lys268, Val270, Val271, Tyr272, Arg273, Ile290	-
Karavilagenin A	Asn54, Val271, Gln79, Trp80, Asp292	-	Thr81
Karavilagenin B	Gln79	Trp80, Tyr263, Leu264, Lys268, Leu210, Arg273, Ile290, Tyr272	-
Karaviloside II	Ser205, Gln79	Trp80, Leu264, Arg273, Leu210, Ile290, Lys268, Tyr263, Tyr272	-
Momordicin I	Val271	Trp80, Lys268, Val270, Leu264, Arg273, Tyr272	-

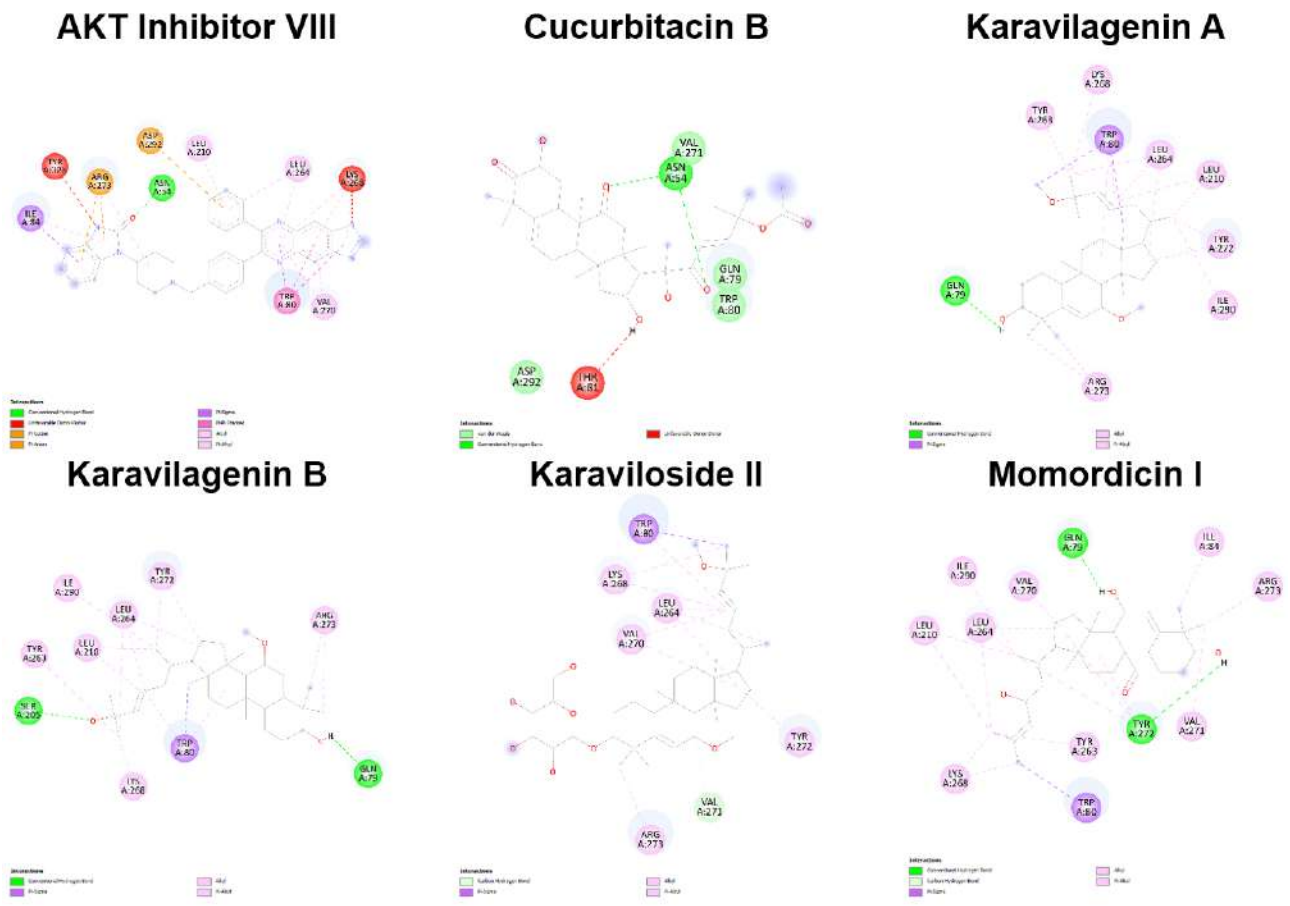


Fig 8. Ligand-protein interaction diagrams of cucurbitane-type triterpenoids within the allosteric binding pocket of AKT1 (PDB: 3O96). Two-dimensional interaction diagrams were generated using BIOVIA Discovery Studio Visualizer. The co-crystallized allosteric inhibitor AKT Inhibitor VIII is shown for comparison. Hydrogen bonds are indicated by green dashed lines, hydrophobic contacts by pink arcs, and other non-covalent interactions as labeled.

Discussion

The present study provides a systems-level perspective on how secondary metabolites of *M. charantia* may influence psoriasis-related biology. The stepwise reduction from 192 reported metabolites to 50 screened compounds indicates that, although bitter melon contains a chemically diverse metabolite profile, only a subset fulfilled the predefined criteria for further pharmacological prioritization. This filtering process narrowed the chemical space to metabolites with comparatively favorable predicted drug-likeness, oral or systemic exposure potential, and preliminary safety profiles. The drug-likeness threshold of ≥0.10 applied in MolSoft was used to exclude compounds with zero or negative scores, retaining natural product scaffolds with positive drug-likeness estimates while allowing subsequent filters to serve as progressively stringent selection steps [23,24]. The bioavailability score threshold of ≥0.55 within the SwissADME system represents the minimum acceptable level across the evaluated pharmacokinetic parameters, excluding compounds with a score of 0.17 that indicate multiple pharmacokinetic liabilities [25]. The Lipinski violation tolerance of fewer than two was applied to accommodate the structural characteristics of terpenoids and steroids, which may deviate marginally from one conventional threshold while retaining acceptable bioavailability [23,24]. Toxicity screening using ADMETlab 3.0 applied a predicted probability threshold of <0.70 for hERG channel blockade and Ames mutagenicity to exclude compounds with predicted safety concerns [26]. Exclusion during screening should not be interpreted as evidence that the remaining metabolites are biologically inactive; rather, they did not meet the operational pharmacokinetic and toxicity criteria applied in this study.

The 50 screened metabolites yielded 347 predicted human targets, of which 159 overlapped with the 3,383 psoriasis-associated genes retrieved from GeneCards. This substantial overlap indicates that many predicted metabolite targets are located within biological networks associated with psoriasis. The finding is consistent with the multifactorial nature of psoriasis, which involves persistent interactions among inflammatory cytokines, epidermal growth regulators, apoptotic pathways, oxidative stress responses, and tissue-remodeling mechanisms [5,6]. Accordingly, the results do not indicate a single dominant mechanism but suggest that *M. charantia* metabolites may influence multiple interconnected components of psoriasis-related biology.

Topological analysis identified AKT1, TNF, EGFR, HIF1A, STAT3, CASP3, PTGS2, MMP9, ESR1, IL1B, and MMP2 as important nodes according to degree and MCC rankings. The recurrence of several genes in both analyses supports their structural importance within the constructed PPI network, although network centrality alone does not establish their functional modulation by the metabolites. These genes are biologically relevant to major pathological features of psoriasis. TNF and IL1B are central mediators of inflammatory amplification in psoriatic skin, driving the recruitment and activation of immune cells and sustaining the cytokine milieu that characterizes active disease [7]. AKT1, EGFR, and STAT3 are involved in keratinocyte proliferation, differentiation, and survival, processes that are dysregulated in psoriatic epidermis [8,36]. CASP3 participates in apoptosis regulation, and its dysregulation contributes to the impaired keratinocyte apoptosis observed in psoriatic plaques [5,6]. HIF1A, MMP9, and MMP2 are associated with microenvironmental adaptation, angiogenesis, and tissue remodeling within psoriatic lesions [5,6]. PTGS2 and ESR1 reflect the involvement of lipid mediator pathways and hormonal-immune interactions in psoriatic pathology [9,10]. Differences between the degree and MCC rankings should not be regarded as contradictory, because degree measures direct connectivity whereas MCC emphasizes participation in densely interconnected subnetworks; the appearance of a gene in both rankings provides stronger evidence of its topological relevance.

The Gene Ontology enrichment profile was consistent with this network-level interpretation. Dominant enriched terms included responses to oxygen-containing compounds, lipids, hormones, peptides, and xenobiotic stimuli, as well as intracellular receptor signaling. These processes are relevant to psoriasis, which is characterized by chronic cytokine-driven inflammation, altered lipid mediators, redox imbalance, and dysregulated signaling in keratinocytes and immune cells [9,10]. The enrichment of terms related to hormonal responses and intracellular receptor signaling may further reflect the involvement of ESR1 and nuclear receptor pathways in immune modulation within psoriatic skin. The term "response to amyloid-beta" warrants cautious interpretation. Its appearance in this analysis most likely reflects the participation of shared inflammatory and cellular stress-response genes, such as those involved in oxidative stress and cytokine signaling, across multiple pathological conditions rather than a psoriasis-specific amyloid mechanism. GO enrichment therefore provides functional hypotheses about the biological processes

engaged by the overlapping target set rather than direct proof of disease-specific mechanisms.

The network and enrichment findings are pharmacologically consistent with previously reported activities of *M. charantia*. Bitter melon and its constituents have demonstrated anti-inflammatory, antioxidant, and immunomodulatory properties [12,13], whereas an ethanolic leaf extract has shown anti-psoriatic activity in a mouse-tail model [14]. The identification of TNF, IL1B, and STAT3 as hub genes provides plausible molecular links to the reported anti-inflammatory effects of the plant. AKT1, EGFR, and CASP3 may connect its metabolites with the regulation of keratinocyte proliferation, survival, and apoptosis, whereas HIF1A and matrix metalloproteinases may relate to redox regulation, microenvironmental responses, and tissue remodeling. These associations provide a possible molecular explanation for previously observed pharmacological effects of bitter melon, although direct modulation of the identified targets by specific metabolites remains to be experimentally demonstrated.

Among the 50 screened metabolites, five cucurbitane-type triterpenoids were selected for molecular docking based on three considerations. First, cucurbitane-type triterpenoids represent the chemotaxonomically distinctive class of secondary metabolites in *M. charantia* and the broader Cucurbitaceae family, differentiating them from widely distributed phytochemicals such as flavonoids and phytosterols that have been extensively studied in other plant systems [12,13]. Second, cucurbitacin B has been experimentally demonstrated to attenuate psoriatic skin lesions and reduce serum levels of IL-6, TNF-alpha, and IL-1beta in an imiquimod-induced mouse model, providing experimental support for the biological relevance of this compound class to psoriasis [15]. Third, the five selected compounds represent structural diversity within the cucurbitane scaffold, including oxygenated cucurbitacins (cucurbitacin B), ring-modified variants (karavilagenin A and B), a glycosidic form (karaviloside II), and an aldehyde-substituted derivative (momordicin I), enabling a preliminary computational exploration of structure-related binding differences within a chemically coherent ligand series. Because the docking analysis was restricted to this representative subset, its findings should be interpreted as a targeted structural follow-up to the network pharmacology results rather than as a comprehensive evaluation of all screened metabolites.

The docking analysis added a structural dimension to the network findings. Redocking of the co-crystallized ligands produced RMSD values below 2.0 Å for all four validated proteins, confirming that the selected docking protocols reproduced the experimentally observed ligand poses within the predefined binding sites. Although PTGS2 was retained as a network-relevant hub gene based on topological analysis, it was excluded from the docking evaluation because preliminary trials produced physically implausible binding energy values for all tested ligands, indicative of technical artifacts. Potential sources include protonation state inconsistencies, charge-assignment artifacts, or structural incompatibility between the cucurbitane scaffold and the evaluated binding pocket. Its relevance to psoriasis biology is not dismissed; however, the docking procedure for this protein requires technical reassessment before structural conclusions can be drawn.

Across the four validated target proteins, AKT1 yielded the most consistently favorable predicted binding energies for all five ligands, with values ranging from -9.30 to -10.86 kcal/mol. These results should be interpreted in the context of the binding pocket used: PDB 3O96 contains AKT Inhibitor VIII, an allosteric inhibitor occupying the interface between the pleckstrin homology (PH) domain and the kinase domain, locking AKT1 in an inactive closed conformation [30,31]. The docking grid was therefore defined around this allosteric pocket rather than the ATP-binding site. Allosteric inhibition at this interface is mechanistically distinct from ATP-competitive inhibition and may confer greater selectivity, as it prevents the membrane-recruitment-dependent conformational activation of AKT1 rather than competing with the high intracellular ATP concentration. The favorable predicted interactions of cucurbitane-type triterpenoids with this pocket may therefore suggest a potential allosteric inhibitory mechanism, although this requires confirmation through binding assays and functional kinase activity studies. AKT1 is a central node in the PI3K/AKT/mTOR signaling axis and has been implicated in keratinocyte proliferation, survival, and resistance to apoptosis in psoriatic skin [36], further supporting its relevance as a docking target in this study.

The convergence between the network and docking findings is particularly notable for AKT1 and EGFR, both of which were identified as topologically important proteins and showed favorable predicted interactions with several tested ligands. EGFR is associated with keratinocyte proliferation and epidermal hyperplasia in psoriasis, and its signaling through the ERK and JNK pathways has been linked to Koebnerization phenomena

in psoriatic skin [8]. IL1B contributes to inflammatory amplification as a central pro-inflammatory cytokine in psoriatic lesions [7]. The combined network and docking findings therefore suggest that selected cucurbitane-type triterpenoids may interact with proteins associated with both the proliferative and inflammatory components of psoriasis, consistent with the multi-target hypothesis generated by the network analysis. However, docking only indicates predicted structural compatibility and does not establish whether a ligand inhibits, activates, or otherwise functionally modulates a target protein.

Interaction analysis using BIOVIA Discovery Studio Visualizer identified specific residues involved in hydrogen bonding and hydrophobic contacts within each binding pocket. For EGFR (1M17), momordicin I and karavilagenin A both engaged the hinge region, sharing the Met769/Lys721 contacts seen with the reference ligand 4-anilinoquinazoline, indicating binding within the canonical ATP-binding cleft. For STAT3 (6NUQ), cucurbitacin B formed hydrogen bonds at Tyr640, Gln644, Lys658, and Ser636 within the SH2 domain, overlapping with key SI-109 contacts and suggesting interference with the same phosphotyrosine-binding pocket. For IL1B (8C3U), momordicin I shared several residues with the reference ligand T9C (notably Asn102, Lys93, and the Val47/Pro57/Val100/Ala115/Met95 hydrophobic cluster), pointing to binding within the same pocket. For AKT1 (3O96), karavilagenin A and cucurbitacin B both engaged Gln79 and Trp80, residues also contacted by AKT Inhibitor VIII, consistent with binding at the allosteric PH domain–kinase domain interface. The extent to which the test compounds shared interacting residues with the co-crystallized ligands provides an indication of whether they engage similar pharmacophoric elements within each binding site, which is relevant to interpreting the predicted binding energies in a structural context.

Among the tested ligands, momordicin I and karavilagenin A showed the most favorable docking profiles. Karavilagenin A produced the most favorable predicted binding energy against AKT1 (-10.86 kcal/mol), whereas momordicin I produced the most favorable values against EGFR (-8.86 kcal/mol) and IL1B (-8.36 kcal/mol). These findings support their prioritization for further experimental investigation. Nevertheless, direct experimental evidence regarding their binding to these specific targets and their anti-psoriatic effects remains absent, and their identification should therefore be regarded as a hypothesis-generating computational finding requiring confirmation through target-specific binding studies, pathway assays, and psoriasis-relevant cellular and animal models.

Cucurbitacin B warrants separate attention because it demonstrated a comparatively consistent predicted interaction profile across multiple psoriasis-related targets, showing favorable binding energies toward AKT1 (-10.60 kcal/mol), IL1B (-7.61 kcal/mol), EGFR (-7.70 kcal/mol), and STAT3 (-7.02 kcal/mol). This cross-target profile is relevant to the multi-target nature of psoriasis. The biological relevance of cucurbitacin B is further supported by prior experimental evidence demonstrating its attenuation of psoriatic lesions and inflammatory markers in an imiquimod-induced mouse model, with proposed involvement of the cGAS-STING pathway [15]. The inflammatory targets identified in the present network analysis, particularly TNF and IL1B, are consistent with the cytokine reductions reported in that study. However, direct binding of Cucurbitacin B to AKT1, EGFR, STAT3, or IL1B was not established in that study; the docking results therefore remain complementary mechanistic hypotheses that require target-specific validation.

Several limitations should be acknowledged. First, the study is entirely computational and generates mechanistic hypotheses rather than experimental proof of pharmacological activity. Second, target prediction and disease-gene retrieval depend on database completeness and may be biased toward extensively studied genes. Third, the screening criteria prioritize predicted oral or systemic drug-like properties but do not establish actual absorption, metabolism, exposure, or safety. Because psoriasis is frequently managed topically, the present screening does not demonstrate suitability for dermal delivery, and additional evaluation of skin permeability, dermal retention, local toxicity, solubility, and formulation compatibility would be required for topical development. Finally, psoriasis is itself a heterogeneous condition with variable immune signatures and clinical phenotypes, and the generalizability of these computational findings across psoriasis subtypes remains to be addressed.

The principal contribution of this study is therefore the reduction of a broad and chemically diverse metabolite pool into a smaller set of compounds and molecular targets that can be evaluated more directly in subsequent experimental studies. The results suggest that *M. charantia* contains metabolites with predicted relevance to inflammatory, proliferative, oxidative stress-related, and tissue-remodeling processes associated

with psoriasis, but they do not demonstrate clinical effectiveness.

Conclusion

Integrated network pharmacology and molecular docking analysis of *M. charantia* secondary metabolites identified 50 compounds fulfilling in silico screening criteria, yielding 159 overlapping targets with psoriasis-associated genes, with AKT1, TNF, EGFR, STAT3, IL1B, CASP3, HIF1A, MMP9, ESR1, and PTGS2 emerging as key network hub genes. Molecular docking of five representative cucurbitane-type triterpenoids against four validated hub proteins demonstrated consistently favorable predicted binding affinities for AKT1 via its allosteric pocket, as well as for EGFR and IL1B, with karavilagenin A, momordicin I, and cucurbitacin B showing the most favorable profiles. These findings collectively support a hypothesis that *M. charantia* may influence psoriasis-related biology through multi-target and multi-pathway mechanisms; however, molecular dynamics simulations, target-specific binding assays, and psoriasis-relevant in vitro and in vivo studies are required to confirm the pharmacological relevance of the prioritized metabolites.

Acknowledgments

The authors thank the Pharmacology Laboratory and the Pharmaceutical Biology Laboratory, Department of Pharmacy, Faculty of Science, Institut Teknologi Sumatera, for providing the computational facilities and technical support used in this study.

Funding

This research was funded by the Ministry of Education, Culture, Research, and Technology of the Republic of Indonesia under the Prototipe grant scheme (contract number 1483b/IT9.2.1/PT.01.03/2025). The funder had no role in study design, data collection and analysis, decision to publish, or preparation of the manuscript.

Declaration of interests

The authors declare that they have no financial or personal relationships with other people or organizations that could inappropriately influence or bias the work reported in this paper.

Author contributions

Conceptualization: ABS, S; Data curation: ABS, MFF, IGRP; Formal analysis: S, ABS, TLN, IGRP; Funding acquisition: S; Investigation: ABS, MFF, IGRP; Methodology: ABS, S; Project administration: S; Supervision: S; Validation: IGRP, TLN; Visualization: TLN, IGRP; Writing – original draft: ABS; Writing – review and editing: S, TLN, NYS, MFF. All authors read and approved the final version of the manuscript.

Received: April 29, 2026
Revised: June 17, 2026
Accepted: June 19, 2026
Published: June 20, 2026

References

1. World Health Organization. Global report on psoriasis. Geneva: World Health Organization; 2016.
2. Armstrong AW, Read C. Pathophysiology, clinical presentation, and treatment of psoriasis: a review. JAMA. 2020;323(19):1945-1960. https://doi.org/10.1001/jama.2020.4006
3. Michalek IM, Loring B, John SM. A systematic review of worldwide epidemiology of psoriasis. J Eur Acad Dermatol Venereol. 2017;31(2):205-212. https://doi.org/10.1111/jdv.13854
4. Damiani G, Bragazzi NL, Karimkhani Aksut C, Wu D, Bragazzi ML, McGonagle D, et al. The global, regional, and national burden of psoriasis: results and insights from the Global Burden of Disease 2019 Study. Front Med (Lausanne). 2021;8:743180. https://doi.org/10.3389/fmed.2021.743180
5. Vičić M, Kaštelan M, Brajac I, Sotošek V, Massari LP. Current concepts of psoriasis immunopathogenesis. Int J Mol Sci. 2021;22(21):11574. https://doi.org/10.3390/ijms222111574
6. Branisteanu DE, Cojocaru C, Diaconu R, Maranduca MA, Branisteanu CI, Stoleriu G, et al. Update on the etiopathogenesis of psoriasis: a review. Exp Ther Med. 2022;23(3):201. https://doi.org/10.3892/etm.2022.11124
7. Cai Y, Xue F, Quan C, Qu M, Liu N, Zhang Y, et al. A critical role of the IL-1beta-IL-1R signaling pathway in skin inflammation and psoriasis pathogenesis. J Invest Dermatol. 2019;139(1):146-156. https://doi.org/10.1016/j.jid.2018.07.025
8. Furue K, Ito T, Tanaka Y, Yumine A, Hashimoto-Hachiya A, Takemura M, et al. The EGFR-ERK/JNK-CCL20 pathway in scratched keratinocytes may underpin Koebnerization in psoriasis patients. Int J Mol Sci. 2020;21(2):434. https://doi.org/10.3390/ijms21020434
9. Cannavò SP, Riso G, Casciaro M, Di Salvo E, Gangemi S. Oxidative stress involvement in psoriasis: a systematic review. Free Radic Res. 2019;53(8):829-840. https://doi.org/10.1080/10715762.2019.1648800

10. Dobrică EC, Cozma MA, Găman MA, Voiculescu VM, Găman AM. The involvement of oxidative stress in psoriasis: a systematic review. Antioxidants (Basel). 2022;11(2):282. https://doi.org/10.3390/antiox11020282
11. Noor F, Tahir ul Qamar M, Ashfaq UA, Albutti A, Alwashmi ASS, Aljasir MA. Network pharmacology approach for medicinal plants: review and assessment. Pharmaceuticals (Basel). 2022;15(5):572. https://doi.org/10.3390/ph15050572
12. Jia S, Shen M, Zhang F, Xie J. Recent advances in Momordica charantia: functional components and biological activities. Int J Mol Sci. 2017;18(12):2555. https://doi.org/10.3390/ijms18122555
13. Bortolotti M, Mercatelli D, Polito L. Momordica charantia, a nutraceutical approach for inflammatory-related diseases. Front Pharmacol. 2019;10:486. https://doi.org/10.3389/fphar.2019.00486
14. Dwarampudi LP, Dhanabal SP, Farha S, Gade R, Shanmugam R, Krishna Raj R. Phytochemical evaluation and anti-psoriatic activity of the ethanolic extract of the leaves of Momordica charantia. Indian J Biochem Biophys. 2022;59(7):751-754.
15. Zhang Y, Wang X, Yang Y, Li J, Chen Y, Cao Y, et al. Cucurbitacin B alleviates skin lesions and inflammation in a psoriasis mouse model by inhibiting the cGAS-STING signaling pathway. Xi Bao Yu Fen Zi Mian Yi Xue Za Zhi. 2025;41(5):428-436.
16. Zhao L, Zhang H, Li N, Chen J, Xu H, Wang Y, et al. Network pharmacology, a promising approach to reveal the pharmacology mechanism of Chinese medicine formula. J Ethnopharmacol. 2023;309:116306. https://doi.org/10.1016/j.jep.2023.116306
17. Eberhardt J, Santos-Martins D, Tillack AF, Forli S. AutoDock Vina 1.2.0: new docking methods, expanded force field, and Python bindings. J Chem Inf Model. 2021;61(8):3891-3898. https://doi.org/10.1021/acs.jcim.1c00203
18. Shamsol Azman ANS, Tan JJ, Abdullah MNH, Bahari H, Lim V, Yong YK. Network pharmacology and molecular docking analysis of active compounds in Tualang honey against atherosclerosis. Foods. 2023;12(9):1779. https://doi.org/10.3390/foods12091779
19. Paggi JM, Pandit A, Dror RO. The art and science of molecular docking. Annu Rev Biochem. 2024;93:389-410. https://doi.org/10.1146/annurev-biochem-030222-120000
20. Pagadala NS, Syed K, Tuszynski J. Software for molecular docking: a review. Biophys Rev. 2017;9(2):91-102. https://doi.org/10.1007/s12551-016-0247-1
21. Kim S, Chen J, Cheng T, Gindulyte A, He J, He S, et al. PubChem 2023 update. Nucleic Acids Res. 2023;51(D1):D1373-D1380. https://doi.org/10.1093/nar/gkac956
22. Khoirunnisa A, Jamil AS, Muchlisin MA. Network pharmacology analysis of secondary metabolites of ciplukan (Physalis angulata L.) against lung cancer. Majalah Farmaseutik. 2024;20(2):282-291. https://doi.org/10.22146/farmaseutik.v20i2.96275
23. Rai M, Singh AV, Paudel N, Jha S, Ghosh S, Patil R, et al. Herbal concoction unveiled: a computational analysis of phytochemicals' pharmacokinetic and toxicological profiles using novel approach methodologies. Curr Res Toxicol. 2023;5:100118. https://doi.org/10.1016/j.crtox.2023.100118
24. Ononamadu CJ, Seidel V. Exploring the antidiabetic potential of Salvia officinalis using network pharmacology, molecular docking, and ADME/drug-likeness predictions. Plants (Basel). 2024;13(20):2892. https://doi.org/10.3390/plants13202892
25. Daina A, Michielin O, Zoete V. SwissADME: a free web tool to evaluate pharmacokinetics, drug-likeness and medicinal chemistry friendliness of small molecules. Sci Rep. 2017;7:42717. https://doi.org/10.1038/srep42717
26. Fu L, Shi S, Yi J, Wang N, He Y, Wu Z, et al. ADMETlab 3.0: an updated comprehensive online ADMET prediction platform enhanced with broader coverage, improved performance, API functionality and decision support. Nucleic Acids Res. 2024;52(W1):W422-W431. https://doi.org/10.1093/nar/gkae236
27. Burley SK, Bhikadiya C, Bi C, Bittrich S, Chao H, Chen L, et al. RCSB Protein Data Bank: powerful new tools for exploring 3D structures of biological macromolecules for basic and applied research and education in fundamental biology, biomedicine, biotechnology, bioengineering and energy sciences. Nucleic Acids Res. 2023;51(D1):D488-D508. https://doi.org/10.1093/nar/gkac1077
28. Stamos J, Sliwkowski MX, Eigenbrot C. Structure of the epidermal growth factor receptor kinase domain alone and in complex with a 4-anilinoquinazoline inhibitor. J Biol Chem. 2002;277(48):46265-46272. https://doi.org/10.1074/jbc.M207135200
29. Huang W, Dong Z, Chen Y, Wang F, Wang CJ, Peng H, et al. Small-molecule inhibitors targeting the DNA-binding domain of STAT3 suppress tumor growth, metastasis and STAT3 target gene expression in vivo. Oncogene. 2016;35(6):783-792. https://doi.org/10.1038/onc.2015.131
30. Barnett SF, Defeo-Jones D, Fu S, Hancock PJ, Haskell KM, Jones RE, et al. Identification and characterization of pleckstrin-homology-domain-dependent and isoenzyme-specific Akt inhibitors. Biochem J. 2005;385(Pt 2):399-408. https://doi.org/10.1042/BJ20041140
31. Mahadevan D, Powis G, Mash EA, George B, Gokhale VM, Zhang S, et al. Discovery of a novel class of AKT pleckstrin homology domain inhibitors. Mol Cancer Ther. 2008;7(9):2621-2632. https://doi.org/10.1158/1535-7163.MCT-08-0243
32. Hanwell MD, Curtis DE, Lonie DC, Vandermeersch T, Zurek E, Hutchison GR. Avogadro: an advanced semantic chemical editor, visualization, and analysis platform. J Cheminform. 2012;4(1):17. https://doi.org/10.1186/1758-2946-4-17
33. Stewart JJP. Optimization of parameters for semiempirical methods V: modification of NDDO approximations and application to 70 elements. J Mol Model. 2007;13(12):1173-1213. https://doi.org/10.1007/s00894-007-0233-4
34. Frisch MJ, Trucks GW, Schlegel HB, Scuseria GE, Robb MA, Cheeseman JR, et al. Gaussian 16, Revision C.01. Wallingford (CT): Gaussian, Inc.; 2019.

35. Forli S, Huey R, Pique ME, Sanner MF, Goodsell DS, Olson AJ. Computational protein-ligand docking and virtual drug screening with the AutoDock suite. Nat Protoc. 2016;11(5):905-919. https://doi.org/10.1038/nprot.2016.051

36. Manning BD, Toker A. AKT/PKB signaling: navigating the network. Cell. 2017;169(3):381-405. https://doi.org/10.1016/j.cell.2017.04.001